Li et al. Nanoscale Research Letters (2017) 12:414
DOI 10.1186/s11671-017-2172-z

Nanoscale Research Letters

NANO EXPRESS Open Access

# Synthesis and Electrochemical Properties of $LiNi_{0.5}Mn_{1.5}O_4$ Cathode Materials with $Cr^{3+}$ and $F^-$ Composite Doping for Lithium-Ion Batteries

Jun Li*, Shaofang Li, Shuaijun Xu, Si Huang and Jianxin Zhu

## Abstract

A $Cr^{3+}$ and $F^-$ composite-doped $LiNi_{0.5}Mn_{1.5}O_4$ cathode material was synthesized by the solid-state method, and the influence of the doping amount on the material's physical and electrochemical properties was investigated. The structure and morphology of the cathode material were characterized by XRD, SEM, TEM, and HRTEM, and the results revealed that the sample exhibited clear spinel features. No $Cr^{3+}$ and $F^-$ impurity phases were found, and the spinel structure became more stable. The results of the charge/discharge tests, cyclic voltammetry (CV), and electrochemical impedance spectroscopy (EIS) test results suggested that $LiCr_{0.05}Ni_{0.475}Mn_{1.475}O_{3.95}F_{0.05}$ in which the $Cr^{3+}$ and $F^-$ doping amounts were both 0.05, had the optimal electrochemical properties, with discharge rates of 0.1, 0.5, 2, 5, and 10 C and specific capacities of 134.18, 128.70, 123.62, 119.63, and 97.68 mAh $g^{-1}$ , respectively. After 50 cycles at a rate of 2 C, $LiCr_{0.05}Ni_{0.475}Mn_{1.475}O_{3.95}F_{0.05}$ showed extremely good cycling performance, with a discharge specific capacity of 121.02 mAh $g^{-1}$ and a capacity retention rate of 97.9%. EIS test revealed that the doping clearly decreased the charge-transfer resistance.

**Keywords:** Solid-state method, Lithium-ion batteries, $LiNi_{0.5}Mn_{1.5}O_4$, Composite doping

## Background

The increasing demand for electric vehicles (EV), hybrid electric vehicles (HEV), and high-capacity storage batteries requires higher performance lithium-ion batteries with improved energy density and power density [1–3]. The cathode material is a key material in lithium-ion batteries, and research and development into high-potential cathode materials is one of the main ways to improve the energy density of lithium-ion batteries. Spinel $LiNi_{0.5}Mn_{1.5}O_4$ has the advantage of discharge voltage plateaus at approximately 4.7 V: low cost, excellent structural stability, and heat stability, and is considered one of the most promising cathode materials for lithium-ion batteries. However, the cycling stability of $LiNi_{0.5}Mn_{1.5}O_4$ is poor, and cycling of this material results in the Jahn-Teller effect and Mn dissolution [4–7].

Modification of the material by doping and coating has been applied to suppress the Jahn-Teller effect and to reduce Mn loss in order to improve the electrochemical properties of the material. Doping modification is a very effective approach that can not only enhance the stability of the crystal structure but also improve the rate capability of the material [8, 9]. During charging, 4.7% of the volume of $LiNi_{0.5}Mn_{1.5}O_4$ is maintained when going from the lithium-rich phase to the lithium-poor phase. The volume change in the material during the insertion/extraction process of Li ions can be effectively suppressed by applying a small amount of doping and surface coating, and furthermore, doping can improve the rate capability and cycling performance of the material [10–12]. Cation doping ( Na [13], Ru [14], Rh [15], Co [16], Al [17], Cr [18], Zn [19], Nd [20], Mg [21], Mo [22], Sm [23], Cu [24], etc.) and anion doping (S [25], P [26], and F [27]) have been applied to modify $LiNi_{0.5}Mn_{1.5}O_4$.

* Correspondence: qhxylijun@gdut.edu.cn
School of Light Industry and Chemical Engineering, Guangdong University of Technology, No.100 Waihuan Xi Road, Guangzhou Higher Education Mega Center, Panyu District, Guangzhou 510006, Guangdong, People's Republic of China

For instance, compared to pure $LiNi_{0.5}Mn_{1.5}O_4$, Al-doped $LiNi_{0.5}Mn_{1.5}O_4$ can effectively improve the discharge capacity (up to 140 mAh $g^{-1}$) and cycling stability (70% capacity retention after 200 cycles) [28].

In this paper, $F^-$ and $Cr^{3+}$ are selected to improve the rate capability via anion-cation compound substitution, and their doping amounts are optimized [29]. In addition, the structure, morphology, and electrochemical properties of the samples were tested and analyzed.

## Methods

The $LiNi_{0.5}Mn_{1.5}O_4$ materials were synthesized by the solid-state method using $Ni(CH_3COO)_2 \cdot 4H_2O$、$Mn(CH_3COO)_2 \cdot 4H_2O$ and $Cr(CH_3COO)_3 \cdot 6H_2O$ as the starting materials.

## Experimental

### Preparation of $LiCr_xNi_{0.5-0.5x}Mn_{1.5-0.5x}O_{3.95}F_{0.05}$

The $LiNi_{0.5}Mn_{1.5}O_4$ materials were synthesized by the solid-state method using $Ni(CH_3COO)_2 \cdot 4H_2O$、$Mn(CH_3COO)_2 \cdot 4H_2O$ and $Cr(CH_3COO)_3 \cdot 6H_2O$ as the starting materials. The materials were fully mixed by ball-milling for 2 h using stoichiometric amounts of $LiCr_xNi_{0.5-0.5x}Mn_{1.5-0.5x}O_{3.95}F_{0.05}$ ($x = 0.025$, 0.05, 0.075), and the dry mixture was heated at 400 °C in air for 5 h. The Ni-Mn-Cr complex oxide formed after natural cooling in a muffle furnace. The obtained complex oxide and lithium source ($Li_2CO_3$ and LiF) were mixed by ball-milling for 4 h using anhydrous alcohol as a dispersant, and the mixture was then heated at 850 °C in air for 12 h to strengthen its crystallization in a muffle furnace. After being reduced at 650 °C in air for 12 h, materials with different $Cr^{3+}$ and $F^-$ composite doping amounts, $LiCr_xNi_{0.5-0.5x}Mn_{1.5-0.5x}O_{3.95}F_{0.05}$ ($x = 0.025$, 0.05, 0.075), were obtained after natural cooling in a muffle furnace.

### Characterization

The crystal structures of the samples were identified by X-ray diffraction (XRD, UltimaIII, diffractometer Cu-Kα radiation, 40 kV, 40 mA, Rigaku, Japan) at room temperature over a 2θ range of 10° to 80° with a scanning speed of 8° $min^{-1}$. The morphology of the $LiCr_xNi_{0.5-0.5x}Mn_{1.5-0.5x}O_{3.95}F_{0.05}$ samples was measured by a scanning electron microscopy (SEM, Hitachi, S-3400N, Japan). The microstructure and elemental composition of the obtained materials were observed by transmission electron microscopy (TEM, Tecnai G2 F20, FEI) equipped with energy dispersive spectroscopy (EDS).

### Electrochemical Performance Test

The electrochemical properties were assessed with CR2032 coin cells, and the cells consisted of the $LiCr_xNi_{0.5-0.5x}Mn_{1.5-0.5x}O_{3.95}F_{0.05}$ electrode as the cathode electrode, Li metal foil as the anode electrode, American Celgard2400 as the separator and 1 mol/L $LiPF_6$ in EC/EMC/DMC (1:1:1 in volume) as the electrolyte. The cathode was synthesized by mixing the active material, carbon black, and polyvinylidene fluoride (PVDF) at a weight ratio of 8:1:1 in the N-methyl pyrrolidinone (NMP) to form a homogeneous slurry, which was then coated on Al foil by a doctor blade coater and subsequently dried in a vacuum oven at 120 °C for 24 h to remove NMP and residual water. The coin cells were assembled in an argon-filled glove box (MBRAUN PRS405/W11006-1, Germany).

The electrochemical performance of $LiCr_xNi_{0.5-0.5x}Mn_{1.5-0.5x}O_{3.95}F_{0.05}$/Li coin cells was evaluated by charging and discharging over 3.5–5.0 V using a CT-300-1A-SA tester (Neware Technology Ltd.). Cyclic voltammograms (CV) tests (the cathode was the working electrode and Li metal foil was both the counter and reference electrode) were carried out using an electrochemical work station (Metrohm Co., Autolab PGSTAT302N, Netherlands) with a scanning rate of 0.1 mV/s and a scanning frequency of 0.5 Hz between 3.5 and 5.0 V. Electrochemical impedance spectroscopy (EIS) was conducted on an electrochemical work station with an AC amplitude of 5 mV in the scanning frequency range of 0.01 to 100 kHz (the cathode was the working electrode and Li metal foil was both the counter and reference electrode ).

## Results and Discussion

Figure 1 shows the XRD pattern of the $LiNi_{0.5}Mn_{1.5}O_4$ and $LiCr_xNi_{0.5-0.5x}Mn_{1.5-0.5x}O_{3.95}F_{0.05}$ ($x = 0.025$, 0.05, 0.075) materials. The pattern revealed that the $Cr^{3+}$ and $F^-$ compound-doped materials had the same diffraction peaks as the undoped sample, suggesting that the samples were synthesized without impurity phases and that $Cr^{3+}$ and $F^-$ compound doping would not change the spinel crystal structure. No impurity peaks or superstructure

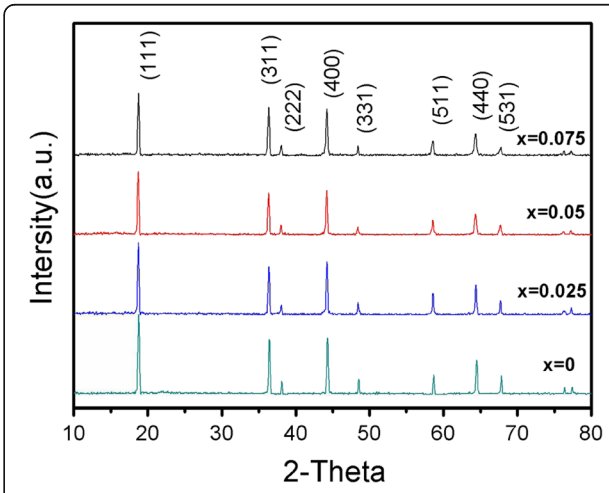


**Fig. 1** XRD patterns of $LiNi_{0.5}Mn_{1.5}O_4$ and $LiCr_xNi_{0.5-0.5x}Mn_{1.5-0.5x}O_{3.95}F_{0.05}$ ($x = 0.025$, 0.05, 0.075)

peaks were found, indicating that some of the $Ni^{2+}$, $Mn^{4+}$, $Mn^{3+}$, and $O^{2-}$ atoms in the spinel phase were successfully substituted by $Cr^{3+}$ and $F^{-}$. The strength of the diffraction peaks of the $Cr^{3+}$-doped $LiCr_xNi_{0.5-0.5x}Mn_{1.5-0.5x}O_{3.95}F_{0.05}$ samples decreased, and excess dopants concentration influenced the degree of crystallinity. The lattice parameters for the $LiNi_{0.5}Mn_{1.5}O_4$ and $LiCr_xNi_{0.5-0.5x}Mn_{1.5-0.5x}O_{3.95}F_{0.05}$ ($x = 0.025, 0.05, 0.075$) materials were calculated by Jade5.0, and the results are shown in Table 1.

Figure 2 shows the SEM images of the $LiNi_{0.5}Mn_{1.5}O_4$ and $LiCr_xNi_{0.5-0.5x}Mn_{1.5-0.5x}O_{3.95}F_{0.05}$ ($x = 0.025$, 0.05, 0.075) with ×10000 magnification. The $LiNi_{0.5}Mn_{1.5}O_4$ sample consists of uniform, submicron-sized particles, and the crystals have a quasi-octahedral shape. After $Cr^{3+}$ and $F^{-}$ compound doping, the $LiCr_xNi_{0.5-0.5x}Mn_{1.5-0.5x}O_{3.95}F_{0.05}$ ($x = 0.025$, 0.05, 0.075) samples exhibited highly crystalline particles and a typical spinels with an octahedral shape and sharp edges and corners.

The existence of chromium and fluoride in the spinel $LiCr_{0.05}Ni_{0.475}Mn_{1.475}O_{3.95}F_{0.05}$ compound was verified by EDS, as shown in Fig. 3. The TEM and high-resolution TEM (HRTEM) images of the crystal morphology and lattice fringes are shown in Fig. 4. Both $LiNi_{0.5}Mn_{1.5}O_4$ and $LiCr_{0.05}Ni_{0.475}Mn_{1.475}O_{3.95}F_{0.05}$ showed similar surface morphologies. The distance between the lattice fringes for $LiNi_{0.5}Mn_{1.5}O_4$ was measured to be 0.4835 nm, corresponding to the (111) plane of spinel. After doping, the lattice spacing in Fig. 4d reveals a value of 0.4811 nm, indicating that the higher bonding energy of Cr-O may shrink the spinel framework. Therefore, $LiCr_{0.05}Ni_{0.475}Mn_{1.475}O_{3.95}F_{0.05}$ is expected to have excellent electrochemical properties for lithium storage.

Figure 5 displays the charge/discharge curves of the $LiNi_{0.5}Mn_{1.5}O_4$ and $LiCr_xNi_{0.5-0.5x}Mn_{1.5-0.5x}O_{3.95}F_{0.05}$ ($x = 0.025$, 0.05, 0.075) samples, where the cells were tested over a potential range of 3.5–5.0 V at a rate of 0.1 C. The discharge specific capacities of the $LiNi_{0.5}Mn_{1.5}O_4$ and $LiCr_xNi_{0.5-0.5x}Mn_{1.5-0.5x}O_{3.95}F_{0.05}$ ($x = 0.025$, 0.05, 0.075) samples were 141.59, 139.38, 134.18, and 124.47 mAh $g^{-1}$ at 0.1 C, respectively. The charge/discharge curve of the doped samples was composed of two obvious voltage plateaus at approximately 4.7 and 4.1 V. The voltage plateau at approximately 4.7 V was attributed to the $Ni^{2+}/Ni^{4+}$ redox couple, while the small voltage plateau at approximately 4.1 V may be due to the substitution of $F^{-}$ for $O^{2-}$, which reduced the amount of negative charge and changed the valence of the transition metal ($Mn^{4+}$ was reduced to $Mn^{3+}$) in order to maintain charge balance.

**Table 1** Refinement results for the samples

| Samples | a/Å |
|---|---|
| $LiNi_{0.5}Mn_{1.5}O_4$ | 8.1775 |
| $LiCr_{0.025}Ni_{0.4875}Mn_{1.4875}O_{3.95}F_{0.05}$ | 8.1803 |
| $LiCr_{0.05}Ni_{0.475}Mn_{1.475}O_{3.95}F_{0.05}$ | 8.1839 |
| $LiCr_{0.075}Ni_{0.4625}Mn_{1.4625}O_{3.95}F_{0.05}$ | 8.1821 |

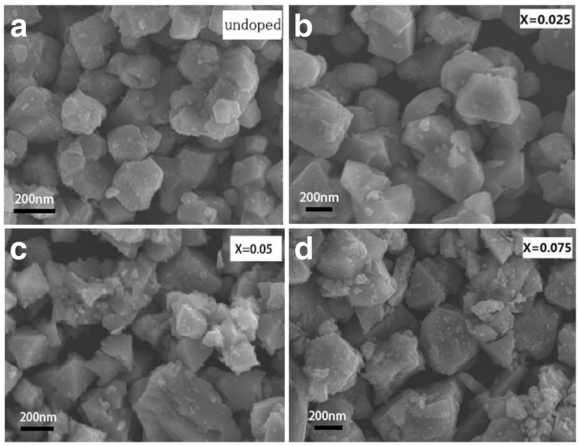


**Fig. 2** SEM images of $LiCr_xNi_{0.5-0.5x}Mn_{1.5-0.5x}O_{3.95}F_{0.05}$.(**a**) $x = 0$, (**b**) $x = 0.025$, (**c**) $x = 0.05$, (**d**) $x = 0.075$

The rate capability is very important for lithium-ion batteries. The cycling performance curves of the $LiNi_{0.5}Mn_{1.5}O_4$ and $LiCr_xNi_{0.5-0.5x}Mn_{1.5-0.5x}O_{3.95}F_{0.05}$ ($x = 0.025$, 0.05, 0.075) samples at different rates are shown in Fig. 6. The highest specific discharge capacity at 0.1 C was observed for $LiNi_{0.5}Mn_{1.5}O_4$ (141.59 mAh $g^{-1}$), and the second highest discharge capacity was observed for $LiCr_{0.025}Ni_{0.4875}Mn_{1.4875}O_{3.95}F_{0.05}$ (139.38 mAh $g^{-1}$). However, at other high rates of 0.5, 2, 5, and 10 C, the specific discharge capacities of the $LiCr_{0.05}Ni_{0.475}Mn_{1.475}O_{3.95}F_{0.05}$ were the highest, which were 128.70, 123.62, 119.63, and 97.68 mAh $g^{-1}$, respectively. When undoped $LiNi_{0.5}Mn_{1.5}O_4$ is discharged at a rate of 2 C , the attenuation of its specific discharge capacity is more obvious. At a discharge rate of 5 C , the structure of the materials may be severely damaged. As the doping amount and substitution of $Cr^{3+}$ increases, the cycling stability increases. A higher doping amount will reduce the specific discharge capacity of the material, making the 4.1 V plateau more obvious and decreasing the energy density of the batteries. On one hand, due to the small polarization at low rate, the polarization effect showed little differences before and after doping. However, the amount of active material decreased after doping, resulting in lower specific capacity. On the other hand, owing to the large polarization at high rate and improved lithium-ion diffusion coefficient, the doped $LiNi_{0.5}Mn_{1.5}O_4$ cathode exhibited higher specific capacity. This result indicates that an appropriate amount of $Cr^{3+}$, $F^{-}$ co-doping can lead to excellent cycling stability and rate capacity.

Figure 7 clearly shows the cycling performance of the $LiNi_{0.5}Mn_{1.5}O_4$ and $LiCr_{0.05}Ni_{0.475}Mn_{1.475}O_{3.95}F_{0.05}$ samples after 50 cycles at 2 C. The initial discharge capacities of $LiCr_{0.05}Ni_{0.475}Mn_{1.475}O_{3.95}F_{0.05}$ and $LiNi_{0.5}Mn_{1.5}O_4$ were

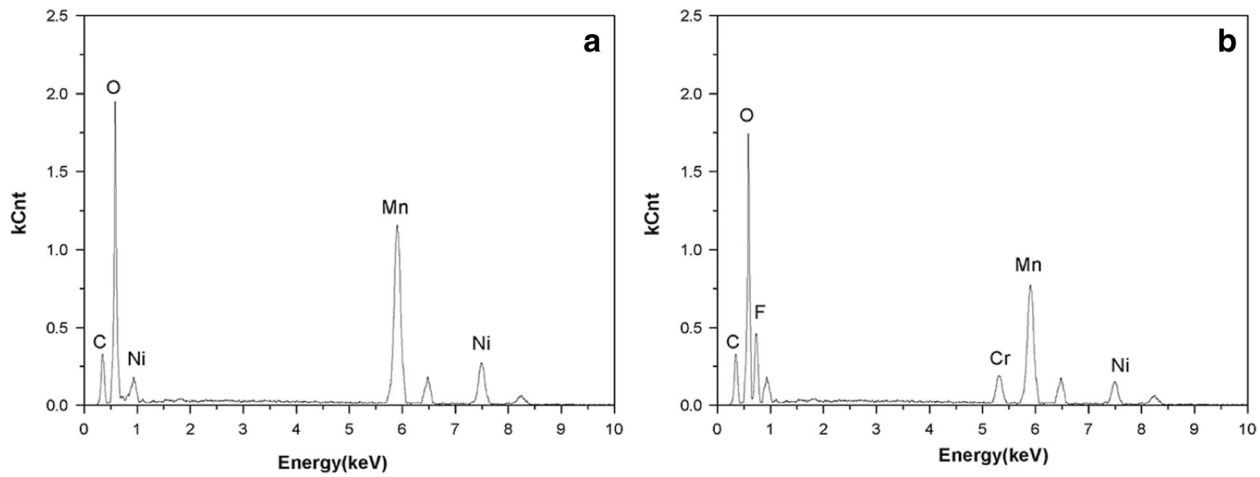


**Fig. 3** EDS patterns of $LiNi_{0.5}Mn_{1.5}O_4$ (**a**) and $LiCr_{0.05}Ni_{0.475}Mn_{1.475}O_{3.95}F_{0.05}$ (**b**)

123.62 and 114.77 mAh $g^{-1}$, respectively, indicating that $LiCr_{0.05}Ni_{0.475}Mn_{1.475}O_{3.95}F_{0.05}$ has a higher initial discharge capacity than undoped $LiNi_{0.5}Mn_{1.5}O_4$. Consequently, $LiCr_{0.05}Ni_{0.475}Mn_{1.475}O_{3.95}F_{0.05}$ could deliver a reversible discharge capacity of 121.02 mAh $g^{-1}$ with a capacity retention of 97.9% after 50 cycles, while $LiNi_{0.5}Mn_{1.5}O_4$ only maintained a reversible discharge capacity of 106.24 mAh $g^{-1}$ with a capacity retention of 92.6%. The capacity retentions of $LiCr_{0.025}Ni_{0.4875}Mn_{1.4875}O_{3.95}F_{0.05}$ and $LiCr_{0.075}Ni_{0.4625}Mn_{1.4625}O_{3.95}F_{0.05}$ were 95.0 and 94.5%, respectively, which indicates that $LiCr_{0.05}Ni_{0.475}Mn_{1.475}O_{3.95}F_{0.05}$ has good capacity retention at high rates among all the samples. The doped material has a higher capacity retention rate due to the bonding energy of Cr-O, which is stronger than the bonding energy of Ni-O and Mn-O and stabilizes the spinel structure. Moreover, the seizing electronic capacity of $F^-$ was stronger and more stable after bonding with Ni, Mn, and Cr, thus improving the stability of the spinel structure. Meanwhile, doping also reduced the erosion of the material by HF in the electrolyte solution and the irreversible loss of active substance during the cycling process. Wang et al. [30] reported that $LiNi_{0.4}Cr_{0.15}Mn_{1.45}O_4$ can deliver a reversible discharge capacity of 139.7 mAh $g^{-1}$ after 40 cycles, corresponding a capacity retention of 97.08%. Li et al. [31] reported the initial discharge capacities of $LiNi_{0.5}Mn_{1.5}O_{3.9}F_{0.1}$ at 0.1, 0.5, 1, 2, and 5 C were 129.07, 123.59, 118.49, 114.49, and 92.57 mAh $g^{-1}$, respectively.

A more detailed analysis of the electrochemical performance was performed by CV and EIS. Figure 8 shows the CV curves of $LiCr_{0.05}Ni_{0.475}Mn_{1.475}O_{3.95}F_{0.05}$ and pure phase $LiNi_{0.5}Mn_{1.5}O_4$. The potential difference of

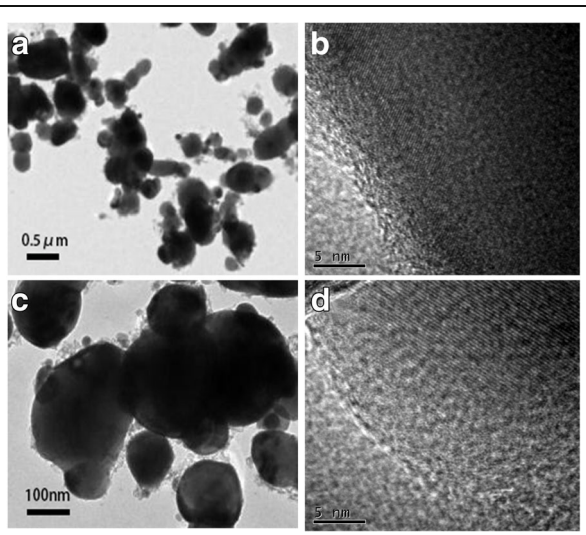


**Fig. 4** TEM and HRTEM images of $LiNi_{0.5}Mn_{1.5}O_4$ (**a** and **b**) and $LiCr_{0.05}Ni_{0.475}Mn_{1.475}O_{3.95}F_{0.05}$ (**c** and **d**)

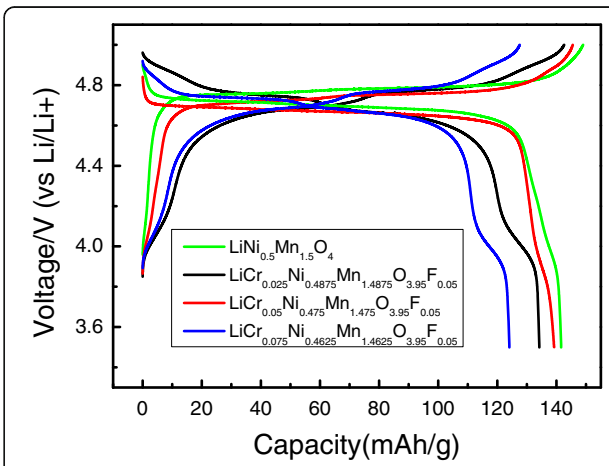


**Fig. 5** Charge/discharge curves of $LiNi_{0.5}Mn_{1.5}O_4$ and $LiCr_xNi_{0.5-0.5x}Mn_{1.5-0.5x}O_{3.95}F_{0.05}$ ($x = 0.025$, 0.05, 0.075) at 0.1 C

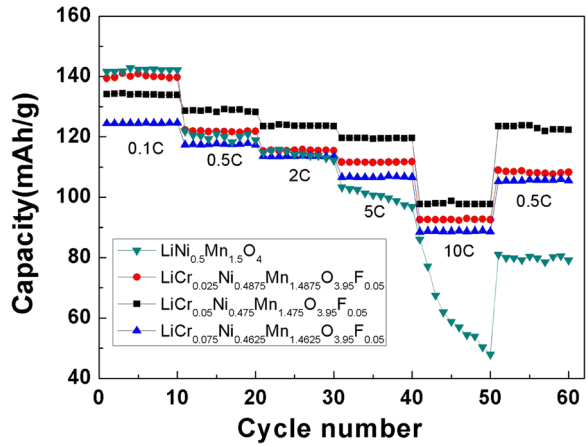


**Fig. 6** Cycling performance of the $LiNi_{0.5}Mn_{1.5}O_4$ and $LiCr_xNi_{0.5-0.5x}Mn_{1.5-0.5x}O_{3.95}F_{0.05}$ ($x = 0.025$, 0.05, 0.075) at different rates

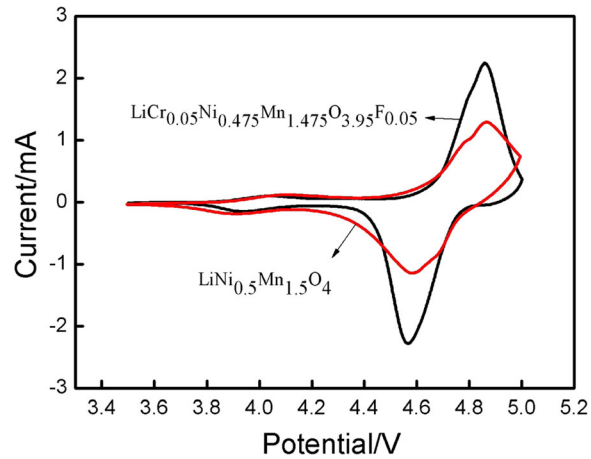


**Fig. 8** Cyclic voltammogram of $LiNi_{0.5}Mn_{1.5}O_4$ and $LiCr_{0.05}Ni_{0.475}Mn_{1.475}O_{3.95}F_{0.05}$

these two materials was 0.298 V. The $LiNi_{0.5}Mn_{1.5}O_4$ oxidation peak potential was 4.861 V, while the reduction peak potential was 4.563 V. The oxidation peak current ($I_{Pa}$) was 2.242 mA, and the reduction peak current ($I_{Pc}$) was 2.288 mA, and thus the $I_{Pa}/I_{Pc}$ ratio was 0.9799. The $LiCr_{0.05}Ni_{0.475}Mn_{1.475}O_{3.95}F_{0.05}$ oxidation peak potential was 4.864 V, the reduction peak potential was 4.578 V, and the potential difference was 0.286 V. The $I_{Pa}$ was 1.273 mA, the $I_{Pc}$ was 1.277 mA, and the $I_{Pa}/I_{Pc}$ ratio was 0.9968 (approximately 1). The above results indicated that the co-doped materials had good reversibility of lithium ions intercalation/deintercalation and improved coulombic efficiency.

Figure 9 shows the EIS patterns of the samples. All the EIS spectra in the figure consist of two semicircles in the high-to-medium frequency region and a sloping line in the low frequency region. The semicircle in the high-frequency region corresponds to lithium ions passing through the electrolyte surface film resistance ($R_s$). The semicircle in the medium frequency region corresponds to the charge-transfer resistance ($R_{ct}$), and the sloping line in the low frequency region is the Warburg impedance ($Z_w$), which is related to lithium ion diffusion in the materials. As seen in Fig. 7, doping decreased the $R_s$, which contributed to improving the diffusivity of lithium ions, the conductivity, and the rate capability of the materials.

The Nyquist plot of the equivalent circuit analog fitted by the ZsimpWin software is shown in Fig. 10. In this circuit, $R_e$ and $R_s$ represent the electrolyte resistance and the particle-to-particle interfacial contact resistance of the SEI film. $R_{ct}$ is the charge-transfer resistance, and $Z_w$ stands for the Warburg impedance caused by diffusion of lithium ions. CPEs and CPEdl

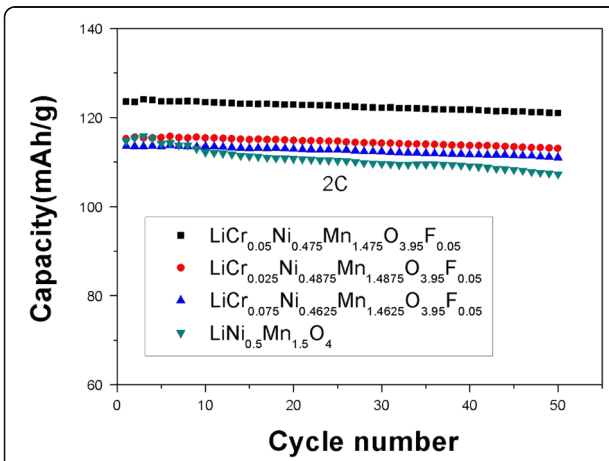


**Fig. 7** Cycling performance of $LiNi_{0.5}Mn_{1.5}O_4$ and $LiCr_xNi_{0.5-0.5x}Mn_{1.5-0.5x}O_{3.95}F_{0.05}$ ($x = 0.025$, 0.05, 0.075) at 2 C

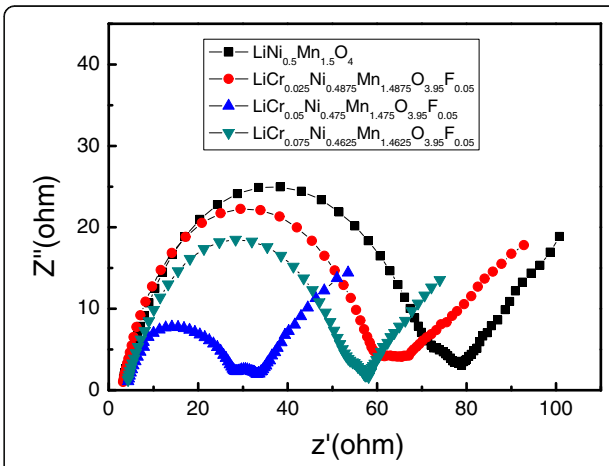


**Fig. 9** EIS patterns of $LiNi_{0.5}Mn_{1.5}O_4$ and $LiCr_xNi_{0.5-0.5x}Mn_{1.5-0.5x}O_{3.95}F_{0.05}$ ($x = 0.025$, 0.05, 0.075)

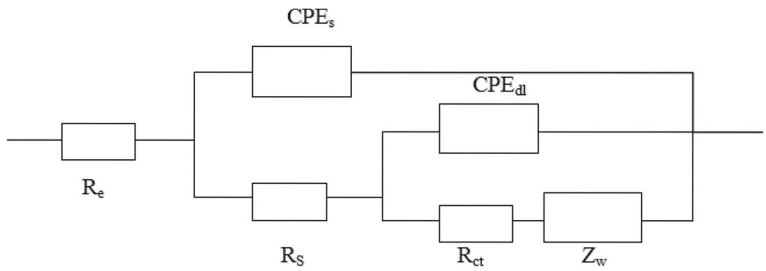


**Fig. 10** The equivalent circuit for the Nyquist plots

are constant phase elements of the solid electrolyte membrane and the double-layer capacitance of the electrode-electrolyte interface, respectively [32]. The fitting parameters of the equivalent circuit analog are summarized in Table 2.

Previous studies have suggested that the diffusion coefficient of lithium ions is associated with the Warburg factor, which can be calculated by the sloping line in the low frequency region. The lithium-ions diffusion coefficient was calculated by Fick's rule using the following equation: [33]

$$D = \frac{R^2 T^2}{2A^2 n^4 F^4 C^2 \sigma^2} \quad (1)$$

where $D$ is the lithium-ion diffusion coefficient, $T$ is the absolute temperature, $R$ is the gas constant, $A$ is the surface area of the electrode, $n$ is the electron transfer number, $F$ is the Faraday constant, $C$ is the molar concentration of lithium ions, and σ is the Warburg factor, which is the slope of the sloping line in Fig. 7.

As seen in Table 2, the $R_s$ values of the doped samples were greatly decreased compared with the undoped sample, and the $R_s$ value of $LiCr_{0.05}Ni_{0.475}Mn_{1.475}O_{3.95}F_{0.05}$ decreased greatly. The decrease in the $R_s$ value indicates that $Cr^{3+}$, $F^-$ co-doping can inhibit the growth of the SEI film to some extent, which may be due to the $F^-$ side reactions between the electrode material and the electrolyte solution. A lower charge-transfer resistance value indicates lower electrochemical polarization, which will lead to higher rate capability and cycling stability. $LiCr_{0.05}Ni_{0.475}Mn_{1.475}O_{3.95}F_{0.05}$ exhibited the lowest $R_{ct}$ value (24.9 Ω) and the highest lithium diffusion coefficient ($1.51 \times 10^{-10}$ cm$^2$ s$^{-1}$) among all the samples, indicating that its electrochemical polarization is the lowest and the lithium-ion mobility of $LiNi_{0.5}Mn_{1.5}O_4$ can be effectively improved by anion-cation compound substitution. EIS also can be used to compare the size of the electronic conductivity. The smaller charge-transfer resistance of the $Cr^{3+}$ and $F^-$ co-doping $LiNi_{0.5}Mn_{1.5}O_4$ indicates a larger electronic conductivity than that of pristine $LiNi_{0.5}Mn_{1.5}O_4$. The electronic conductivity of $LiNi_{0.5}Mn_{1.5}O_4$ is about $3.88 \times 10^{-5}$ S cm$^{-1}$, while the electronic conductivities of $LiCr_xNi_{0.5-0.5x}Mn_{1.5-0.5x}O_{3.95}F_{0.05}$ ($x = 0.025$, 0.05, 0.075) samples were $6.19 \times 10^{-5}$ S cm$^{-1}$, $1.25 \times 10^{-4}$ S cm$^{-1}$, and $5.98 \times 10^{-5}$ S cm$^{-1}$, respectively. In fact, $LiCr_{0.05}Ni_{0.475}Mn_{1.475}O_{3.95}F_{0.05}$ has the best electrochemical performance among all four samples. The decrease in $R_{ct}$ and the increase in $D$ indicate that the proper amount of $Cr^{3+}$, $F^-$ co-doping has a positive effect on the electrochemical reaction activity of the material.

**Table 2** Fitting parameters of the Nyquist plots for the samples

| Samples | Rs/Ω | Rct/Ω | D/cm$^2$ s$^{-1}$ |
|---|---|---|---|
| $LiNi_{0.5}Mn_{1.5}O_4$ | 5.2 | 70.3 | $1.05 \times 10^{-11}$ |
| $LiCr_{0.025}Ni_{0.4875}Mn_{1.4875}O_{3.95}F_{0.05}$ | 7.9 | 57.6 | $5.48 \times 10^{-11}$ |
| $LiCr_{0.05}Ni_{0.475}Mn_{1.475}O_{3.95}F_{0.05}$ | 2.9 | 24.9 | $1.51 \times 10^{-10}$ |
| $LiCr_{0.075}Ni_{0.4625}Mn_{1.4625}O_{3.95}F_{0.05}$ | 4.3 | 50.2 | $4.49 \times 10^{-11}$ |

## Conclusions

The $Cr^{3+}$, $F^-$ co-doped analog of $LiNi_{0.5}Mn_{1.5}O_4$ ($LiCr_xNi_{0.5-0.5x}Mn_{1.5-0.5x}O_{3.95}F_{0.05}$ ($x = 0.025$, 0.05, 0.075)) was synthesized by the high-temperature solid-state method. The materials's XRD patterns showed that $Cr^{3+}$ and $F^-$ successfully substituted some of the $Ni^{2+}$, $Mn^{4+}$, $Mn^{3+}$, and $O^{2-}$ atoms in the spinel material, and no impurity peaks existed. The specific discharge capacities of $LiCr_{0.05}Ni_{0.475}Mn_{1.475}O_{3.95}F_{0.05}$ at 0.1, 0.5, 2, 5, and 10 C were 134.18, 128.70, 123.62, 119.63, and 97.68 mAh g$^{-1}$, respectively. The specific discharge capacity was 121.02 mAh g$^{-1}$ after 50 cycles at 2 C, which is of 97.9% the initial discharge capacity. The capacity retention rate of $LiCr_{0.05}Ni_{0.475}Mn_{1.475}O_{3.95}F_{0.05}$ was the largest among the samples. The materials had good crystallinity, and the largest number of octahedral spinel was well distributed. $Cr^{3+}$, $F^-$ co-doped of the materials significantly improved the specific discharge capacity at higher rate, improved the cycling stability, enhanced the reversibility of lithium ions, and reduced the impedance value.

**Acknowledgements**
This work was supported by the National Natural Science Foundation of China (No. 20672023), the Science and Technology Plan Foundation of Guangzhou (201704030031) and the Science and Technology Plan Foundation of Guangdong (2015A050502046).

**Authors' Contributions**
The idea is from JL, the manuscript was mainly written by SL and SH, and the figures were mainly drawn by SX and JZ. All authors read and approved the final manuscript.

**Competing Interests**
The authors declare that they have no competing interests.

**Consent for Publication**
Not applicable.

**Ethics Approval and Consent to Participate**
Not applicable.

## Publisher's Note
Springer Nature remains neutral with regard to jurisdictional claims in published maps and institutional affiliations.

Received: 22 March 2017 Accepted: 30 May 2017
Published online: 15 June 2017

**References**
1. Hu M, Pang XL, Zhou Z (2013) Recent progress in high-voltage lithium ion batterie. J Power Sources 237:229–242.
2. Xue NS, Du WB, Greszler TA, Shyy W, Martins JRRA (2014) Design of a lithium-ion battery pack for PHEV using a hybrid optimization method. Appl Energy 115:591–602.
3. Qian YY, Fu YS, Wang X, Xia H (2014) $LiNi_{0.5}Mn_{1.5}O_4$ nanorod clusters as cathode material for high energy and high power lithium-Ion batteries. J Nanosci Nanotechno 14:7038–7044.
4. Seyyedhosseinzadeh H, Mahboubi F, Azadmehr A (2013) Diffusion mechanism of lithium ions in $LiNi_{0.5}Mn_{1.5}O_4$. Electrochim Acta 108:867–875.
5. Liu YZ, Zhang MH, Xia YG, Qiu B, Liu ZP, Li X (2014) One-step hydrothermal method synthesis of core-shell $LiNi_{0.5}Mn_{1.5}O_4$ spinel cathodes for Li-ion batteries. J Power Sources 256:66–71.
6. Chong J, Xun SD, Song XY, Liu G, Battaglia VS (2013) Surface stabilized $LiNi_{0.5}Mn_{1.5}O_4$ cathode materials with high-ratecapability and long cycle life for lithiumion batteries. Nano Energy 2:283–293.
7. Tang X, Jan SS, Qian YY, Xia H, Ni JF, Savilov SV, Aldoshin SM (2015) Graphene wrapped ordered $LiNi_{0.5}Mn_{1.5}O_4$ nanorods as promising cathode material for lithium-ion batteries. Sci Rep 5:11958.
8. Yi TF, Xie Y, Ye MF, Jiang LJ, Zhu RS, Zhu YR (2011) Recent developments in the doping of $LiNi_{0.5}Mn_{1.5}O_4$ cathode material for 5V lithium-ion batteriers. Ionics 17:383–389.
9. Liu GY, Kong X, Sun HY, Wang BS (2014) Extremely rapid synthesis of disordered $LiNi_{0.5}Mn_{1.5}O_4$ with excellent electrochemical performance. Ceram Int 40:14391–14395.
10. Leitner KW, Wolf H, Garsuch A, Chesneau F, Schulz-Dobrick M (2013) Electroactive separator for high voltage graphite/$LiNi_{0.5}Mn_{1.5}O_4$ lithium ion batteries. J Power Sources 244:548–551.
11. Wang W, Liu H, Wang Y, Zhang J (2013) Effects of chromium doping on performance of $LiNi_{0.5}Mn_{1.5}O_4$ cathode material. T Nonferr Metal Soc 23: 2066–2070.
12. Xia H, Tang SB, Lu L, Meng YS, Ceder G (2007) The influence of preparation conditions on electrochemical properties of $LiNi_{0.5}Mn_{1.5}O_4$ thin film electrodes by PLD. Electrochim Acta 52:2822–2828.
13. Wang J, Lin WQ, Wu BH, Zhao JB (2014) Syntheses and electrochemical properties of the Na-doped $LiNi_{0.5}Mn_{1.5}O_4$ cathode materials for lithium-ion batteries. Electrochim Acta 145:245–253.
14. Wang H, Tan TA, Yang P, Lai MO, Lu L (2011) High-rate performances of the Ru-doped spinel $LiNi_{0.5}Mn_{1.5}O_4$ : effects of doping and particle size. The J Phy Chem C 115:6102–6110.
15. Wu P, Zeng XL, Zhou C, Gu GF, Tong DG (2013) Improved electrochemical performance of $LiNi_{0.5-x}Rh_xMn_{1.5}O_4$ cathode materials for 5V lithium ion batteries via Rh-doping. Mater Chem Phys 138:716–723.
16. Ito A, Li D, Lee Y, Kobayakawa K, Sato Y (2008) Influence of Co substitution for Ni and Mn on the structural and electrochemical characteristics of $LiNi_{0.5}Mn_{1.5}O_4$. J Power Sources 185:1429–1433.
17. Zhong GB, Wang YY, Zhang ZC, Chen CH (2011) Effects of Al substitution for Ni and Mn on the electrochemical properties of $LiNi_{0.5}Mn_{1.5}O_4$. Electrochim Acta 56:6554–6561.
18. Mao J, Dai K, Xuan M, Shao G, Qiao R, Yang W, Battaglia VS, Liu G (2016) Effect of chromium and niobium doping on the morphology and electrochemical performance of high-voltage spinel $LiNi_{0.5}Mn_{1.5}O_4$ cathode material. ACS Appl Mater Interfaces 8:9116–9124.
19. Yang Z, Jiang Y, Kim J, Wu Y, Li G, Huang Y (2014) The $LiZn_xNi_{0.5-x}Mn_{1.5}O_4$ spinel with improved high voltage stability for Li-ion batteries. Electrochim Acta 117:76–83.
20. Yi T, Yin L, Ma Y, Shen H, Zhu Y, Zhu R (2013) Lithium-ion insertion kinetics of Nb-doped $LiMn_2O_4$ positive-electrode material. Ceram Int 39:4673–4678.
21. Alcántara R, Jaraba M, Lavela P, Tirado JL, Zhecheva E, Stoyanova R (2004) Changes in the local structure of $LiMg_yNi_{0.5-y}Mn_{1.5}O_4$ electrode materials during lithium extraction. Chem Mater 16:1573–1579.
22. Yi TF, Chen B, Zhu YR, Li XY, Zhu RS (2014) Enhanced rate performance of molybdenum-doped spinel $LiNi_{0.5}Mn_{1.5}O_4$ cathode materials for lithium ion battery. J Power Sources 247:778–785.
23. Mo M, Hui KS, Hong XT, Guo JS, Ye CC, Li AJ, Hu NQ, Huang ZZ, Jiang JH, Liang JZ, Chen HY (2014) Improved cycling and rate performance of Sm-doped $LiNi_{0.5}Mn_{1.5}O_4$ cathode materials for 5V lithium ion batteries. Appl Surf Sci 290:412–418.
24. Yang M, Xu B, Cheng J, Pan C, Hwang B, Meng YS (2011) Electronic, structural, and electrochemical properties of $LiNi_xCu_yMn_{2-x-y}O_4$ ($0 < x < 0.5$, $0 < y < 0.5$) high-voltage spinel materials. Chem Mater 23:2832–2841.
25. Sun Y, Oh SW, Yoon CS, Bang HJ, Prakash J (2006) Effect of sulfur and nickel doping on morphology and electrochemical performance of $LiNi_{0.5}Mn_{1.5}O_{4-x}S_x$ spinel material in 3-V region. J Power Sources 161:19–26.
26. Deng Y, Zhao S, Xu Y, Gao K, Nan C (2015) Impact of P-doped in Spinel $LiNi_{0.5}Mn_{1.5}O_4$ on degree of disorder, grain morphology, and electrochemical performance. Chem Mater 27:7734–7742.
27. Ming H, Ming J, Oh S, Tian S, Zhou Q, Huang H, Sun Y, Zheng J (2014) Surfactant-assisted synthesis of $Fe_2O_3$ nanoparticles and F-doped carbon modification toward an improved $Fe_3O_4$@$CF_x$/$LiNi_{0.5}Mn_{1.5}O_4$ battery. ACS Appl Mater Interfaces 6:15499–15509.
28. Liu XL, Li D, Mo QL, Guo XY, Yang XX, Chen GX, Zhong SW (2014) Facile synthesis of aluminum-doped $LiNi_{0.5}Mn_{1.5}O_4$ hollow microspheres and their electrochemical performance for high-voltage Li-ion batteries. J Alloys Compd 609:54–59.
29. Xiao J, Chen X, Sushko PV, Sushko ML, Kovarik L, Feng J, Deng Z, Zheng J, Graff GL, Nie Z, Choi D, Liu J, Zhang J, Whittingham MS (2012) High-performance $LiNi_{0.5}Mn_{1.5}O_4$ spinel controlled by $Mn^{3+}$ concentration and site disorder. Adv Mater 24:2109–2116.
30. Wang SJ, Li P, Shao LY, Wu KQ, Lin XT, Shui M, Long NB, Wang DJ, Shu J (2015) Preparation of spinel $LiNi_{0.5}Mn_{1.5}O_4$ and Cr-doped $LiNi_{0.5}Mn_{1.5}O_4$ cathode materials by tartaric acid assisted sol–gel method. Ceram Int 41: 1347–1353.
31. Li J, Li QB, Li SF, Zhu JX, Liu JJ (2017) Synthesis and performance study of F-doped $LiNi_{0.5}Mn_{1.5}O_4$ cathode material. Rare Metal Mat Eng 46:339–444.
32. Yi TF, Xie Y, Zhu YR, Zhu RS, Ye MF (2012) High rate micron-sized niobium-doped $LiMn_{1.5}Ni_{0.5}O_4$ as ultra high power positive-electrode material for lithium-ion batteries. J Power Sources 211:59–65.
33. Das SR, Majumder SB, Katiyar RS (2005) Kinetic analysis of the $Li^+$ ion intercalation behavior of solution derived nano-crystalline lithium manganate thin films. J Power Sources 139:261–268.